THE JOURNAL OF BIOLOGICAL CHEMISTRY
Vol. 279, No. 1, Issue of January 2, pp. 495–508, 2004
Printed in U.S.A.

Protein Profile of Tax-associated Complexes*

Received for publication, September 10, 2003
Published, JBC Papers in Press, October 6, 2003, DOI 10.1074/jbc.M310069200

Kaili Wu‡, Maria Elena Bottazzi§, Cynthia de la Fuente‡, Longwen Deng‡, Scott D. Gitlin¶, Anil Maddukuri‡, Shabnam Dadgar‡, Hong Li‖, Akos Vertes, Anne Pumfery‡ ‡‡, and Fatah Kashanchi‡ ‡‡§§**

*From the Departments of ‡Biochemistry and Molecular Biology and §Microbiology and Tropical Medicine, School of Medicine and Health Sciences, The George Washington University, Washington, D. C. 20037, ‖Department of Biochemistry and Molecular Biology, University of Medicine and Dentistry, New Jersey Medical School, Newark, New Jersey 07103, ¶Department of Internal Medicine, Division of Hematology/Oncology, University of Michigan, Ann Arbor, Michigan 48109-0640, and **Department of Chemistry, The George Washington University, Washington, D. C. 20052*

Infection with human T-cell leukemia virus type 1 (HTLV-1) results in adult T-cell leukemia and HTLV-1-associated myelopathy/tropical spastic paraparesis. Tax, a 40-kDa protein, regulates viral and cellular transcription, host signal transduction, the cell cycle, and apoptosis. Tax has been shown to modulate cellular CREB and NFκB pathways; however, to date, its role in binding to various host cellular proteins involved in tumorigenesis has not been fully described. In this study, we describe the Tax-associated proteins and their functions in cells using several approaches. Tax eluted from a sizing column mostly at an apparent molecular mass of 1800 kDa. Following Tax immunoprecipitation, washes with high salt buffer, two-dimensional gel separation, and mass spectrometric analysis, a total of 32 proteins was identified. Many of these proteins belong to the signal transduction and cytoskeleton pathways and transcription/chromatin remodeling. A few of these proteins, including TXBP151, have been shown previously to bind to Tax. The interaction of Tax with small GTPase-cytoskeleton proteins, such as ras GAP^{1m}, Rac1, Cdc42, RhoA, and gelsolin, indicates how Tax may regulate migration, invasion, and adhesion in T-cell cancers. Finally, the physical and functional association of Tax with the chromatin remodeling SWI/SNF complex was assessed using *in vitro* chromatin remodeling assays, chromatin remodeling factor BRG1 mutant cells, and RNA interference experiments. Collectively, Tax is able to bind and regulate many cellular proteins that regulate transcription and cytoskeletal related pathways, which might explain the pleiotropic effects of Tax leading to T-cell transformation and leukemia in HTLV-1-infected patients.

Infection with human T-cell leukemia virus type 1 (HTLV-1)[1] results in adult T-cell leukemia and HTLV-1-associated myelopathy/tropical spastic paraparesis. The Tax protein encoded by HTLV-1 plays a central role in the development of both adult T-cell leukemia and HTLV-1-associated myelopathy/tropical spastic paraparesis. Although Tax itself does not bind to DNA directly or function as an enzyme, its ability to regulate multiple cellular responses is conferred by its protein-protein interactions with various host cellular factors. Importantly, HTLV-1-mediated activation of the host T-cell is induced primarily by the viral protein Tax, which influences transcriptional activation, signal transduction, cell cycle control, and apoptosis. Therefore, understanding how Tax controls these pathways is of significant importance. Tax targets several transcriptional pathways including CREB/activating transcription factor, NFκB, and multiple other factors including cell cycle regulators, such as cyclins D2 and D3, the mitotic checkpoint regulator MAD1, the cyclin-dependent kinases (Cdk) Cdk4 and Cdk6, Cdk inhibitors (p16/INK4A and p21/Waf1), and the tumor suppressor p53 (1). Moreover, Tax regulation is observed at both nuclear (*e.g.* CREB-dependent) and cytoplasmic (*e.g.* NFκB-dependent) levels, functioning through shuttling proteins between these two compartments (2, 3).

To activate transcription of the HTLV-1 genome, nuclear Tax interacts with the CREB/activating transcription factor family of transcriptional activators, which bind to the viral long terminal repeat (LTR). The interaction of Tax with CREB and the CREB response elements in the LTR results in a CREB response element-CREB-Tax ternary complex (4). Tax also directly binds to the KIX domain of the transcriptional co-activators CREB-binding protein (CBP) and p300 (5). CBP and p300 covalently modify (acetylate) substrates such as histones and transcription factors and may serve as integrators of numerous cellular signaling processes with the basal RNA polymerase II machinery (3, 6, 7, 45). This would, in turn, allow controlled regulation and interaction with many cellular transcription factors including CREB, NFκB/Rel, p53, c-Myb, c-Jun, c-Fos, and transcription factor IIB in a signal-dependent and, sometimes, mutually exclusive fashion.

Equally important among Tax-binding proteins is the persistent activation of NFκB by Tax, which contributes to the initiation and maintenance of the malignant phenotype. Cytoplasmic Tax interferes with the NFκB pathway via a direct Tax/

* This work was supported in part by National Institutes of Health Grants AI44357, AI43894, and 13969 (to F. K.), by the Alexandrine and Alexander Sinsheimer Foundation (to K. W., H. L., and L. D.), and by Research Enhancement Fund 111501 from The George Washington University (to A. V. and F. K.). The costs of publication of this article were defrayed in part by the payment of page charges. This article must therefore be hereby marked "*advertisement*" in accordance with 18 U.S.C. Section 1734 solely to indicate this fact.

‡‡ These authors contributed equally to this work.
§§ To whom correspondence should be addressed: Dept. of Biochemistry and Molecular Biology, School of Medicine, Ross Hall, Rm. 552, The George Washington University, 2300 Eye St., NW, Washington, D. C. 20037. Tel.: 202-994-1782; Fax: 202-994-1780; E-mail: bcmfxk@gwumc.edu.

[1] The abbreviations used are: HTLV-1, human T-cell leukemia virus type 1; CREB, cAMP-response element-binding protein; NFκB, nuclear factor-κB; Cdk, cyclin-dependent kinase; LTR, long terminal repeat; CBP, CREB-binding protein; 2-D, two-dimensional; BAF, BRG-associated factor; DTT, dithiothreitol; IP, immunoprecipitation; MM, molecular mass; MALDI-TOF, matrix-assisted laser desorption ionization time-of-flight; ChIP, chromatin IP; WT, wild type; HA, hemagglutinin; siRNA, small interfering RNA; TNF-α, tumor necrosis factor-α; MS, mass spectrometry; RNAi, RNA interference; JNK, c-Jun N-terminal kinase; MEKK, mitogen-activated protein kinase/extracellular signal-regulated kinase kinase kinase. IKK, IκB kinase; IEF, isoelectric focusing; TNE, Tris-NaCl-EDTA.

IKK interaction, which leads sequentially to chronic IKK activation, continuous IκB turnover, and persistent NFκB activity (8). Genetic complementation analyses with IKKγ-deficient rat fibroblast cells that fail to activate NFκB in the presence of Tax suggested that IKKγ is required for the assembly of the Tax-responsive IKK complex (9). IKKγ functions as a molecular adapter and provides a site for Tax binding in the assembly of Tax/IKK complexes. IκB kinase activity can be reconstituted *in vivo* by over-expressing Tax, IKKγ, and either IKKα or IKKβ. However, interaction of Tax with IKKα and IKKβ does not induce kinase activity in the absence of IKKγ expression (10). These interactions with Tax require sequences in the C-terminal region of IKKγ whereas the N-terminal region of IKKγ is required for the formation of a stable and active holo-IKK complex (11–14).

The function of tax primarily relies on protein-protein interactions. Potential binding sites on the Tax polypeptide have been determined previously (3, 14, 15) through mutation analysis of various amino acid residues. For example, both N-terminal and C-terminal domains are responsible for CREB binding (15, 16) and IKKγ binding (3, 14). In addition, amino acids 81 to 95 of Tax are required for p300/CBP interaction (17). The dimerization of Tax, which relies on the leucine repeats, results in a more active protein as compared with its monomeric form (14, 18). Furthermore, Chun *et al.* (19) demonstrated that a few of the targets of Tax share coiled-coil structures and that the same domain of Tax is responsible for interaction with different coiled-coil proteins.

Here, we have attempted to determine and define Tax-binding proteins using chromatography, 2-D gel electrophoresis, and mass spectrometric analysis. Through these proteomic approaches, we have identified new proteins that bound to Tax, some of which operate with small GTPases, and control many well known cytoskeleton proteins. We also have identified nuclear-containing Tax complexes containing chromatin remodeling factors such as BRG1 and BRG-associated factors (BAFs), which remodel resident nucleosomes. Finally, through the use of a "conserved domain" BLAST search, we demonstrate that Tax contains many overlapping structures and domains, including a LIM binding domain, a coiled-coil region, an ERM domain, and a myosin tail-like domain, which could account for the ability of Tax to act at both the nuclear and cytoplasmic level.

EXPERIMENTAL PROCEDURES

Cell Culture and Cell Extract Preparation

Cell culture was performed as described previously (20). C8166 (C81) is an HTLV-1-infected T-cell line, and CEM (12D7) is an uninfected human T-cell line established from patients with T-cell leukemia. All cells were cultured in RPMI 1640 containing 10% fetal bovine serum, 1% streptomycin/penicillin, and 1% L-glutamine (Quality Biological) at 37 °C and in 5% CO_2. MT-2 and HUT102 cells are HTLV-1-infected T-cells producing viral particles and are positive for Tax expression. JPX-9 is a Tax-inducible (Cd^{2+}) cell line. Whole cell extracts were made at 30 mg/ml, as determined by the Coomassie Blue and BCA (Bio-Rad) protein assay method and were used in chromatography and subsequent immunoaffinity/Western blot analysis. Aliquoted extracts were kept at −80 °C in 10% glycerol for later use.

Expression of GST fusion proteins was performed in *Escherichia coli* transformed with GST-Cdc42, -RhoA, -Rac1, and -Tax plasmids (a generous gifts from Dr. Richard A. Cerione, Dept. of Molecular Medicine, Cornell University, Ithaca, NY). Sonicated lysates were treated as described previously and added to a 30% slurry of glutathione-Sepharose beads (Amersham Biosciences) (20). Reduced glutathione was added to elute fusion proteins, which were dialyzed against 2 liters of Transcription Buffer D. Tax protein was purified by differential precipitation and zinc chelate chromatography as described previously (21).

Size Exclusion Chromatography

Gel filtration was conducted on an AKTA Purifier system (Amersham Biosciences) with a Superose 6 10/30 column. One ml of C81 lysate (protein concentration, 30 mg/ml) was applied to the column each time. Samples were eluted with Buffer D (20 mM HEPES, pH 7.9, 0.05 M KCl, 0.2 mM EDTA, 0.5 mM phenylmethylsulfonyl fluoride, 0.05 M DTT, and 20% glycerol; Quality Biological, Inc.) plus 600 mM NaCl at a flow rate of 0.4 ml/min. Eluates were monitored by absorbency at 280 nm. Fractions were collected at 0.5 ml in individual tubes. Standard molecular masses (aldolase, catalase, ferritin, tryroglobulin, and blue dextran 2000, from Amersham Biosciences) were applied to the column and ran under the same conditions as the C81 extracts to calculate the size and range of each fraction.

In Vitro Bindings Assays

Anti-Tax polyclonal antibody was raised in rabbits as described previously (20). Polyclonal antibodies against BAF53, BAF57, BAF155, and BRG1 were generous gifts from Dr. Weidong Wang (Laboratory of Genetics, NIA, National Institutes of Health, Baltimore, MD). Other antibodies were purchased from Santa Cruz Biotechnology, Inc. (Santa Cruz, CA) including annexin VI, actin, Cdc42, cyclin D2, GAP^{1m}, gelsolin, p21, βpak, PCTAIRE-1, Rad51, and RAG2, from Upstate Biotechnology (CDK2), and from Calbiochem (p53 (Ab-1)). Each antibody was diluted 1:1000 in TNE buffer for Western blot analysis.

Immunoprecipitation (IP)—Aliquots of cell extracts or fractions from gel filtration were incubated with various antibodies overnight at 4 °C followed by addition of 30% (v/v) protein A-protein G-agarose beads (Oncogene Research Products, Boston, MA). Bound complexes were washed three times with 150, 300, or 1000 mM NaCl in 100 mM Tris-HCl solution, pH 7.5, containing 1 mM EDTA and 0.1% Nonidet P-40. A final wash was performed with 50 mM NaCl/Tris-HCl with 0.1% Nonidet P-40. For washes with 1000 mM salt solution, the protein A/G beads were also treated with 1% bovine serum albumin (in the same solution) for 20 min and washed with buffer without bovine serum albumin. As a control for 2-D gel electrophoresis, a parallel IP experiment was performed at the same time with IgG antibodies. The washed samples were used for electrophoresis on either SDS-PAGE or IEF/SDS-PAGE (2-D).

Pull-down Assay—Two micrograms of GST-Rac1, GST-Cdc42, GST-RhoA, GST-Tax, or purified GST proteins were mixed with 1 mg of various lysates (CEM or C81). Aliquots of 30% glutathione-Sepharose beads were then added to the reaction mixture at a total volume of 200–300 μl and rocked overnight at 4 °C. The next day, bound complexes were washed three times with 600 mM NaCl in 100 mM Tris-HCl solution, pH 7.3, containing 1 mM EDTA and 0.1% Nonidet P-40 and subsequently washed in 50 mM NaCl/100 mM Tris-HCl. Beads were dissociated in loading buffer prior to SDS-PAGE.

For concentrating column fractions and subsequent Western blotting, an equal volume of 20% trichloroacetic acid was added to the protein solutions. After incubation for 30 min at 4 °C, the mixture was centrifuged to obtain pellets, followed by two washes with 0.4 ml of cold acetone (two times). Supernatants were removed, and the pellets were dried by high speed vacuum at 4 °C and used in SDS-PAGE analysis.

Electrophoresis and Western Blot

One-dimensional SDS-PAGE—SDS-PAGE was carried out as described (22) with a pre-cast gradient gel (4–20%; Invitrogen). After electrophoresis, gels were either stained with Coomassie Blue R-250 or silver staining reagent (Bio-Rad) or were transferred to polyvinylidene difluoride membrane for Western blot analysis.

Two-dimensional Gel Electrophoresis (IEF/SDS-PAGE)—Two-dimensional gel electrophoresis was performed according to the method of O'Farrell (23) as follows: isoelectric focusing was carried out in glass tubes with an inner diameter of 2.0 mm using 2.0%, pH 3.5–10, ampholines (Amersham Biosciences) for 9600 V-h. Fifty ng of an IEF internal standard (tropomyosin with a molecular mass of 33 kDa and pI of 5.2) was added to the sample solution as an internal control. The pH gradient plot for this set of ampholines was determined with a surface pH electrode. After equilibration for 10 min in 62.5 mM Tris-HCl buffer, pH 6.8, including 50 mM DTT, 2.3% SDS, 10% glycerol, each tube gel was sealed at the top of a stacking gel, which was put on top of a 10% acrylamide slab gel (0.75 mm thick, 17 × 14 cm). SDS slab gel electrophoresis was carried out for about 4 h at 12.5 mA/gel. Standard molecular mass proteins were added to a well near the basic edge. After electrophoresis, the gel was stained by the silver staining method of O'Connell and Stults (24) and dried between two sheets of cellophane.

For Western blots, protein samples were separated on SDS-PAGE and then transferred to an Immobilon-P (polyvinylidene difluoride;

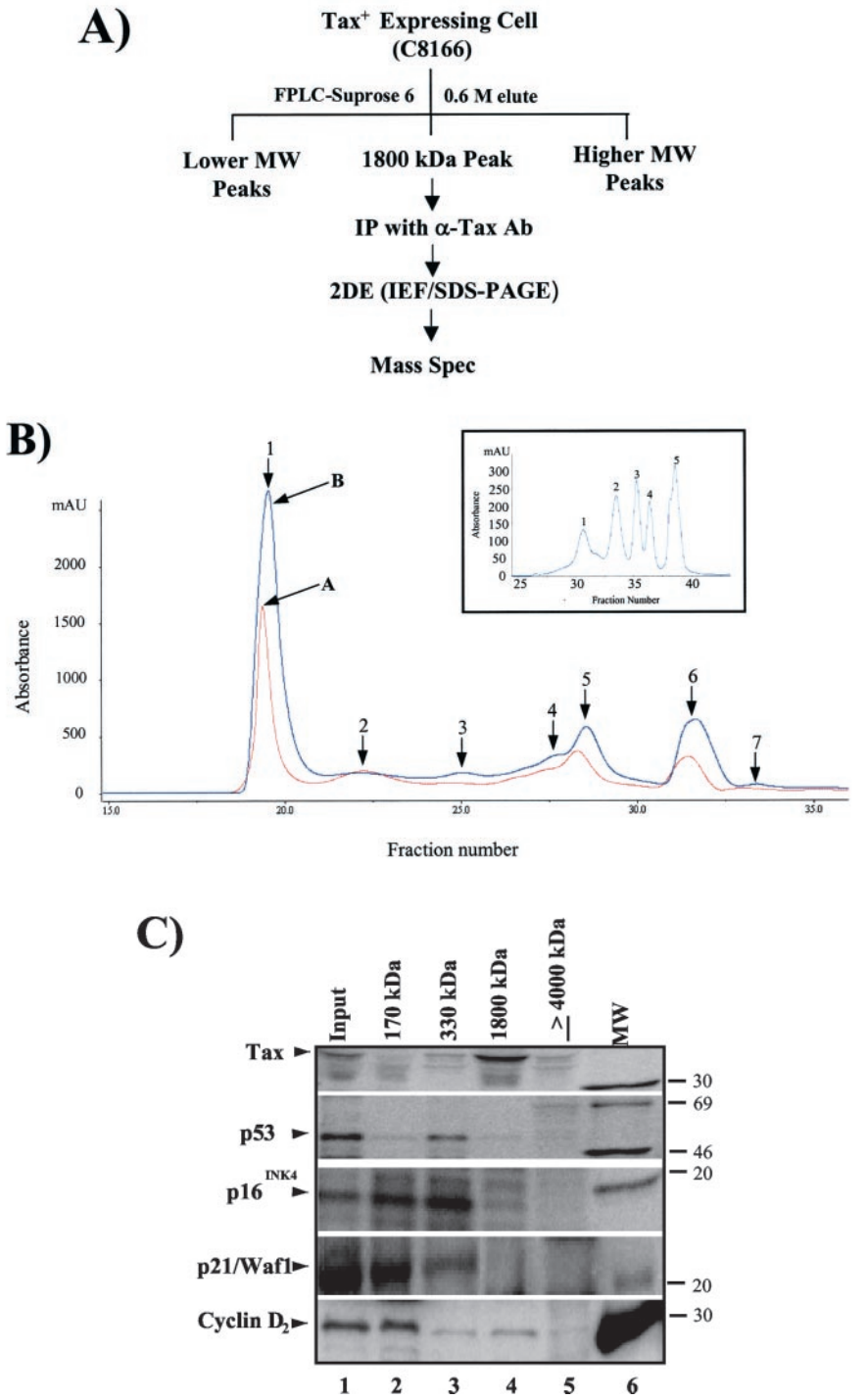

FIG. 1. **A general approach for purification of various Tax-associated proteins.** *A*, schematic flow diagram for separation and identification of Tax-associated proteins. Samples were loaded onto a sizing column (Superose 6 10/30 column) and separated in the presence of 600 mM salt. Selected apparent molecular mass complexes were further used for either IP or Western blots as seen in *panel C*. *B*, standard protein markers (*inset*) with apparent molecular masses ranging from 158 to 2,000 stokes radius values were initially used to calibrate the size of protein peaks. Various apparent protein peaks were observed including dextran blue 2000 (*peak 1*, MM 2000), tryroglobulin (*peak 2*, MM 670), ferritin (*peak 3*, MM 440), catalase (*peak 4*, MM 232), and aldolase (*peak 5*, MM 158). Subsequently, C81 extracts were chromatographed with either 600 mM salt (*A peaks*) or 150 mM salt (*B peaks*) over the Superose 6 sizing column. Seven different peaks were apparent with either salt concentration when using C81 extracts. *Fraction 1* is the largest complex and *fraction 7* is the smallest. *C*, presence of Tax and cell cycle-related proteins in various fractions from size exclusive chromatography (size range from 170 to >4,000 kDa). Each *lane* represents TCA-precipitated proteins (0.5 ml fraction, 0.05 to 0.15 mg total protein), which were washed with acetone and run on a 4–20% SDS-PAGE for Western blot with anti-polyclonal Tax, p53, p16, p21, and cyclin D2 antibodies. C81 cell extracts were used as positive controls for Western blots in *lane 1* (*Input*). The majority of Tax appears in the 1800-kDa fraction. The size of each fraction was calculated according to standard proteins (see "Experimental Procedures"), which were run under the same 600 mM salt conditions.

Millipore) membrane and blocked with 5% fat-free milk (in TNE_{50}/0.1% Nonidet P-40). Membranes were incubated overnight with various primary antibodies. Reactive complexes were developed with protein G-labeled ^{125}I and visualized with a PhosphorImager scanner (Amersham Biosciences) (20).

MALDI-TOF Analysis

Individual protein spots were excised from the silver-stained gel and destained with a solution of 30 mM potassium ferricyanide/100 mM sodium thiosulfate (1:1) (v/v). Trypsin-digested sample solutions were further desalted and concentrated with C18 ZipTips (Millipore). Samples were mixed with the same volume of the matrix solution (α-cyano-4-hydroxycynnamic acid in 50% acetonitrile/0.1% (v/v) trifluoroacetic acid). Two μl of the mixtures were applied to the sample plate and introduced into the mass spectrometer after drying. Mass spectra were recorded in the reflectron mode of a MALDI-TOF mass spectrometer (Voyager-Elite; PerSeptive Biosystems) by summing 200–300 laser shots with an acceleration voltage of 20 kV, 70% grid voltage, 0.05 guide wire voltage, 100-ns delay, and low mass gate at 700 *m/z*.

Data Base Analysis

Proteins were identified using the peptide mass fingerprinting analysis software ProFound (129.85.19.192/prowl-cgi/ProFound.exe). The NCBInr data base was used for the searches with several passes of searching with different limitations for each spot. In general, all spots were searched with methionine oxidation and no-limitation for pI. The best match for each spot was considered with higher coverage rate, more matched peptides, and higher score without limitation on the taxonomic category and protein mass. Zero missed cleavage by trypsin and lowest mass tolerance, *i.e.* ±50 ppm, were considered for most of the proteins. A few spots were searched with the following parameters to find the best match: two missed cut cleavages, limited to the "mammal" category, and/or a set ±50% of total molecular mass (see website for more details). We consistently used various multiple parameters

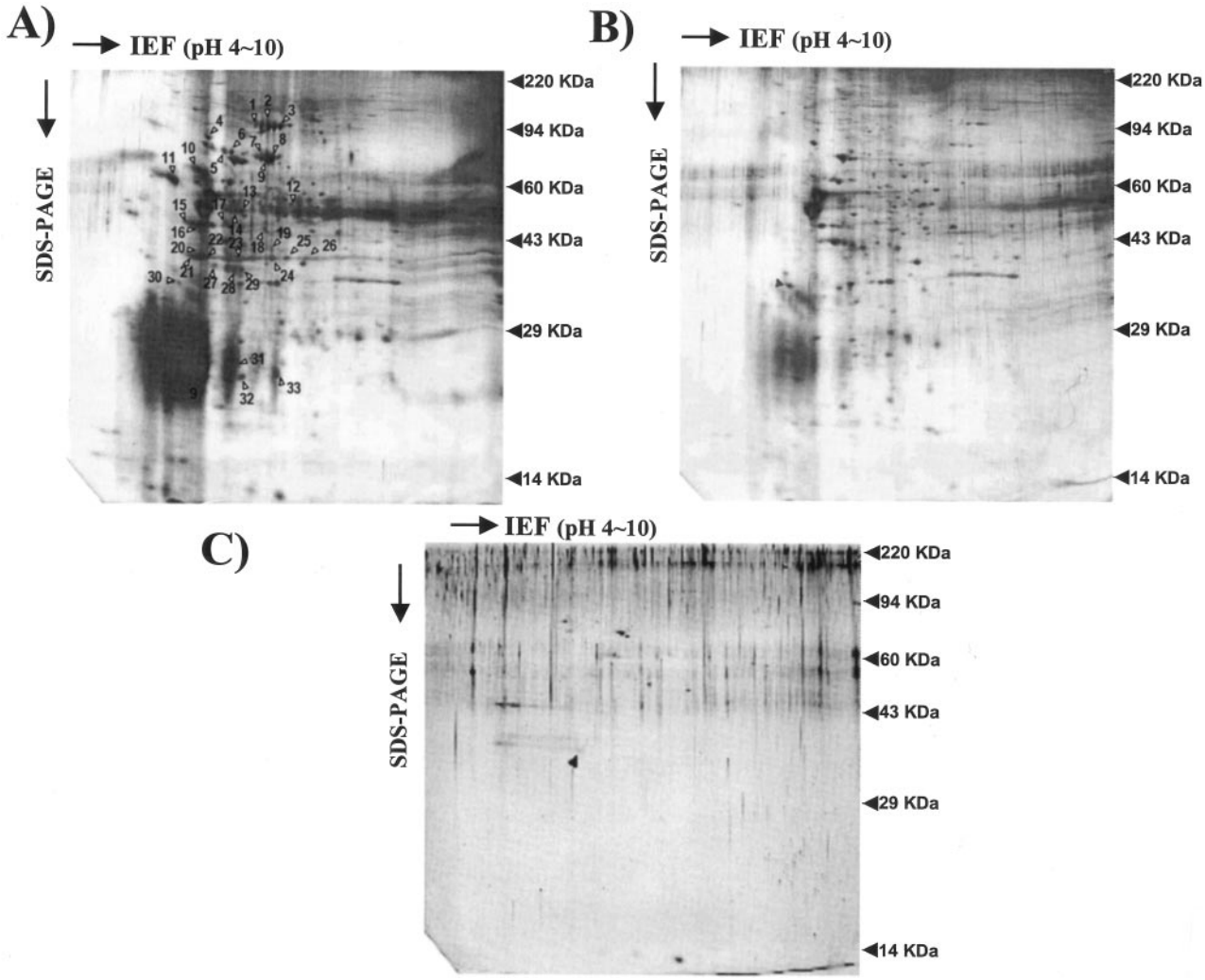

FIG. 2. **Two-dimensional electrophoresis pattern of the Tax 1800-kDa fraction and MALDI-TOF MS analysis of associated proteins.** The 1800-kDa fraction was immunoprecipitated with anti-Tax polyclonal antibody (*A*), IgG pre-immune antibody as control (*B*), or beads alone with no antibody (*C*). The original gel size was 17 × 14 × 0.75 cm. Proteins were detected by silver staining. Molecular mass calibration was performed using reference markers (indicated on the *right-hand side*). The pI was measured directly by a surface pH electrode. The *numbers* indicated on the *left gel* represent spots that were unique and reproducible as compared with the control gel. Identification of spots and their corresponding numbers are listed in Table II as identified by MALDI-TOF MS analysis. *Spot 30* in *panel A* and *small arrows* in *panel B* and *C* are tropomyosin and were used as an internal standard control. *D*, typical MALDI-TOF mass spectra of in-gel digested sample spots (*1*, *2*, *4*, *6*, *7*, *16*, *19*, and *25*) from 2-D PAGE. *Star*-labeled peaks of each spectrum (Table I) are peptides matched for specific protein candidates found in the data base.

such as low miss cut, low ppm, first methionine oxidation, and others in our searches to obtain more reliably matched proteins. Identification of the proteins was confirmed by Western blot analysis.

Unless stated specifically, all data bases and tools used for bioinformatics analysis were from the following public websites: PubMed, www.ncbi.nlm.nih.gov/PubMed/; ExPASy, us.expasy.org/; BLAST, www.ncbi.nlm.nih.gov/BLAST/; Pfam, pfam.wustl.edu/; PBIL, pbil.univ-lyon1.fr/pbil.html; COILS, www.ch.embnet.org/software/COILS_form.html; and PIR, www-nbrf.georgetown.edu/pirwww/.

In Vitro Chromatin Remodeling Assay

Plasmid pG5E4T DNA (five Gal4 binding sites upstream of the adenovirus 2 E4 minimal promoter) was linearized with Asp-718. The fragments were biotinylated, gel purified, and reconstituted with core histones by step dilution. Briefly, core histones were purified from HeLa cells and mixed with DNA. The biotinylated mononucleosome were prepared by mixing the biotinylated pG5E4T DNA and purified core histones by sequential dilution from 1 to 0.1 M NaCl. Ten to twenty micrograms of pG5E4T PCR products were mixed with 5 μl of 5 M NaCl and 2 μl of 10× reconstitution buffer (0.15 M Tris-HCl, pH 7.5, 1 mM DTT, 2 mM EDTA) by pipetting up and down repeatedly. Next 30–40 μg of core histones were added in a total volume of 50 μl, adjusting the volume by adding distilled deionized water. Samples were then gently flicked in the tube and incubated at 37 °C for 20 min. Sequential dilution was carried out by adding 10 μl of 1× reconstitution buffer every 10 min, for 3 h at 37 °C. At each time point, samples were mixed by gently pipetting up and down. An aliquot was run on an agarose gel to ensure proper nucleosome assembly prior to each experiment. The biotinylated nucleosomal arrays were then incubated at 30 °C for 1 h with paramagnetic beads coupled to streptavidin in a binding buffer containing 10 mM HEPES, pH 7.8, 50 mM KCl, 5 mM DTT, 5 mM phenylmethylsulfonyl fluoride, 5% glycerol, 0.25 mg/ml bovine serum albumin, and 2 mM $MgCl_2$, supplemented with 300 mM KCl. Following the standard ChIP protocol (25) modified for *in vitro* conditions (26), 100 nM Gal4-VP16, 200 nM Gal4, 200 nM Gal4-Tax (M47), or Gal4-Tax (WT) were added to ~500 ng of biotinylated nucleosomal array in 20 μl of binding buffer (4.2 nM) and incubated for 30 min at 30 °C. Twenty-five nM SWI/SNF and 10-fold excess of competitor chromatin was then added. After 30 min of incubation at 30 °C, formaldehyde was added to 1% of the final reaction volume and incubated for 15 min at room temperature. The templates were then released from biotin and the Dynabeads by digestion with restriction enzyme at 37 °C for 4 h. Samples were digested with 10 milliunits of MNase in 3 mM $CaCl_2$ for 5 min at room temperature. The samples were then immunoprecipitated using affinity matrix HA antibody to pull-down SWI/SNF and the cross-linked DNA. The beads were washed, and cross-linking was reversed by adding 5 M NaCl. DNA was extracted by proteinase K digestion, phenol-chloroform extraction, and ethanol precipitation. The denatured samples were applied to Zeta-probe membranes by slot blot and hybridized to successive probes of 250–300 bp generated by PCR and labeled by

D)

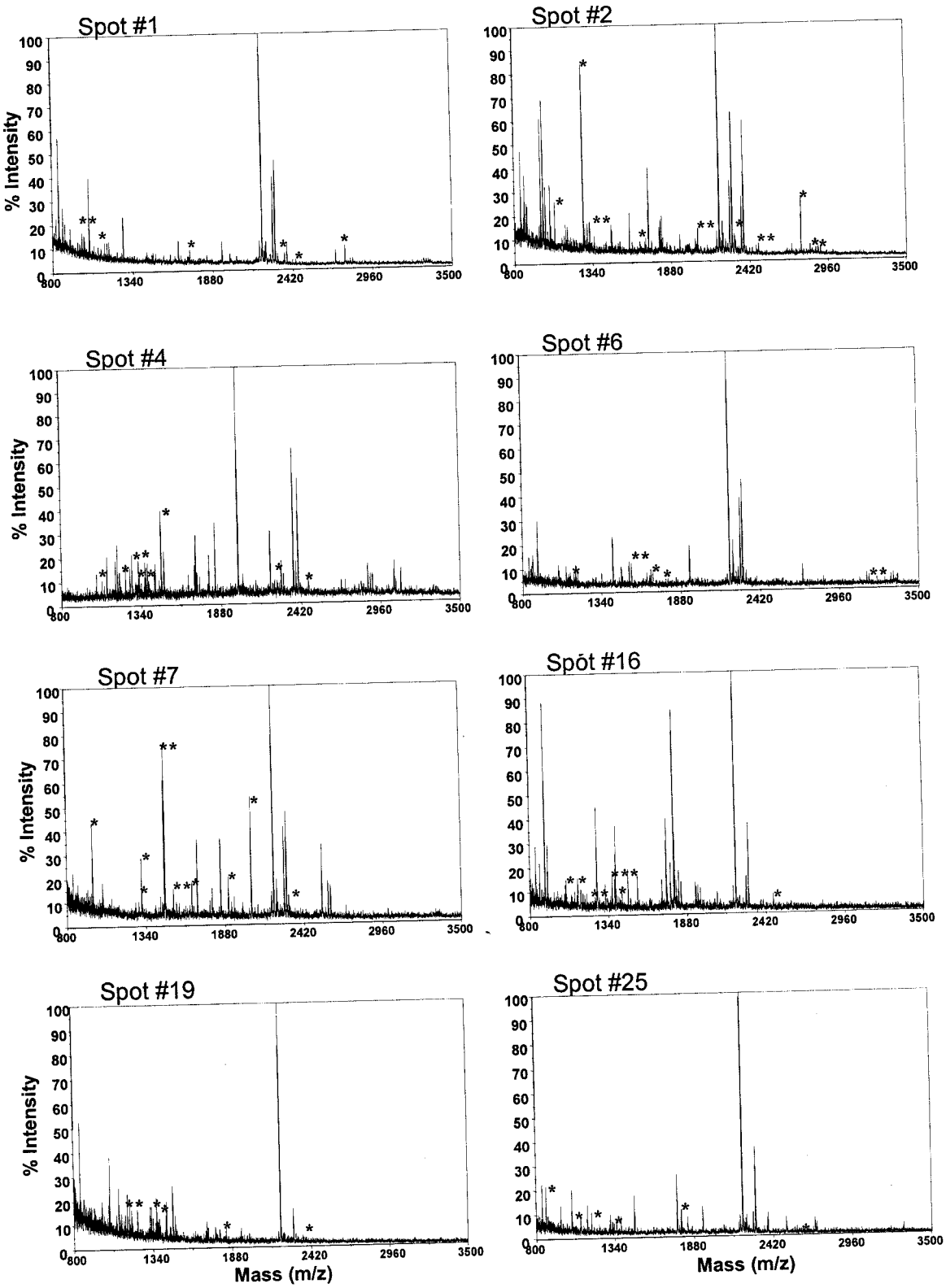

FIG. 2—*continued*

random hexanucleotide primer extension (Roche Applied Science).

To ensure the presence of chromatin structure in our reconstitution assays, we used micrococcal nuclease digestion of plasmid pG5E4T DNA. Chromatin was analyzed by digesting 2000 ng (20 μl) at each time point with 5 units of micrococcal nuclease per microliter and 0.3 mM $CaCl_2$ for 0, 0.5, 1, and 5 min at room temperature. Reactions were stopped with 8 μl of 2.5% Sarkosyl-0.1 M EDTA. Proteins were then digested overnight at 37 °C with 10 μl of 10 mg/ml proteinase K and 0.2% SDS. Following an ethanol precipitation, DNA was analyzed on a 1.2% agarose gel.

siRNA Analysis

Oligos were designed and synthesized using the OligoEngine website at www.oligoengine.com and the accession number for BRG1. Five oligos (see below), which span the 5′ end, middle, and 3′ end of the BRG1 mRNA, were chosen. The most optimal sequences had a GC content between 30 and 70%. HTLV-1-infected cell lines, C91/PL and MT-2, were treated with TNF-α for 2 h. A mixture of the five oligos was electroporated (27) into the cells, and HTLV-1 replication was monitored by p19/gag enzyme-linked immunosorbent assay. The sequences of oligos used for BRG1 siRNA (wild type) were as follows: U29175–1716, GGACAAGCGCCUGGCCUAC; U29175–2142, GAAGAUUCCAGAUCCAGAC; U29175–3210, GAUCUGCAACCACCCCUAC; U29175–4236, GCAGUGGCUCAAGGCCAUC; U29175–4776, GGAGGAUGACAGUGAAGGC. The sequences used for BRG1 siRNA (mutant) were as follows: U29175–1716, GGACAAAAAAAAUGGCCUAC; U29175–2142, GAAGAUUCCAAAAAAAGAC; U29175–3210, GAUCUGCAACCAAAAAUAC; U29175–4236, GCAGUGGCUCAAAAAAAUC; U29175–4776, GGAGGAUGAAAAAAAAGGC.

RESULTS

Generally, there are two strategies for high throughput proteome analysis of protein samples prepared from cells or tissues. Two-dimension gel electrophoresis (IEF/SDS-PAGE, 2-D) displays and quantifies proteins from 10 to 100 kDa. The identification of spots on 2-D gels is usually performed by in-gel trypsin digestion combined with MALDI-TOF and/or electrospray ionization mass spectrometry (MS). Another approach fragments protein samples with trypsin, followed by separation of peptides using liquid chromatography, which directly interfaces with the mass spectrometer. In the present study, we first focused on determining the components of Tax associated complexes in HTLV-1-infected cells using fractionation on a sizing column, followed by immunoprecipitation with anti-Tax polyclonal antibody, 2-D gel electrophoresis, and identification of associated polypeptides by MALDI-TOF analysis (Fig. 1*A*).

Extracts from HTLV-1-infected lymphocyte cell lines were separated using a size-exclusion column. The extracts were equilibrated to high salt (600 mM) concentrations of eluate to wash out nonspecific Tax-binding proteins. Standard protein markers (*inset* in Fig. 1*B*) with apparent molecular masses ranging from 158 to 2,000 stokes radius values were initially used to calibrate the size of protein peaks. Various apparent protein peaks were observed including dextran blue 2000 (peak 1, MM 2000), tryroglobulin (peak 2, MM 670), ferritin (peak 3, MM 440), catalase (peak 4, MM 232), and aldolase (peak 5, MM 158). When applying the infected cell lysates to the column, there were at least seven peaks with apparent molecular masses ranging from 30 kDa to more than 4,000 kDa. Consistent with a previously published report (28), one of the peaks contained Tax associated with IKKs (28). However, the Tax eluted at three sizes with the majority found in peak 5 (apparent molecular mass of 1800 kDa). The results of fractionations at high salt (600 mM, *A*) and low salt (150 mM, *B*) are shown in Fig. 1*B*. Either condition essentially showed similar peak profiles. We focused on one particular fraction, the 1800-kDa fraction, because it was reproducibly observed in four different HTLV-1- and Tax-expressing cells (C8166, MT-2, HUT 102, and JPX-9; data not shown). As controls for fractionation, several other factors important in HTLV-1 pathology (p53, $p16^{INK4}$, p21/Waf1, and cyclin D2) were also detected in fractions of C8166 (C81) cells by Western blotting (Fig. 1*C*). The positive bands for cyclin D2 (an activator of the cell cycle), p21/Waf1 and $p16^{INK4}$ (both inhibitors of the cell cycle), and p53 (a cell cycle regulator) appeared in lower molecular mass fractions, *i.e.* 170 and 330 kDa (*lanes 1* and *2*).

The apparent molecular mass 1800-kDa fraction was further used for IPs with anti-Tax antibodies. Four available monoclonal antibodies (Tabs 69, 70, 71, and 72) were used for immunoprecipitations; however, none of the monoclonal antibodies alone, or the combination of all four antibodies combined, showed a consistent pattern of Tax immunoprecipitation from C81 cells (data not shown). Next, polyclonal rabbit anti-Tax antibodies were used for immunoprecipitation analysis. Isolated complexes from polyclonal rabbit anti-Tax immunoprecipitates were separated by 2-D gel electrophoresis and silver stained. Compared with a control pre-immune IP (Fig. 2*B*), unique spots on a 2-D gel were observed following an anti-Tax IP and suggested that Tax bound to a number of cellular proteins (Fig. 2*A*). A control IP with no antibodies was also used in pull-down assays (Fig. 2*C*). Unique spots that bound to Tax were excised, digested with trypsin, and subjected to MALDI-TOF analysis (Fig. 2*D*). Peptide sequences of some of the spots are listed in Table I.

Data base searches (BLAST, www.ncbi.nlm.nih.gov/BLAST/; Pfam, pfam.wustl.edu/) suggested several protein candidates, which are listed in Table II (spot 30, tropomyosin, is an internal standard for 2-D PAGE). Six proteins (spots 9, 10, 16, 18, 24, and 25) in Table II belong to a kinase family or contained a conserved kinase domain. At least two protein candidates had Zn-finger structures (spots 6 and 17), ten were related to the small GTPase-cytoskeleton pathway (spots 1, 2, 3, 5, 9, 10, 14, 21, 23, and 31), and at least one component of the SWI/SNF chromatin remodeling complex was found to bind to Tax (spot 18). One of the identified proteins, TXBP151 (spot 5), has been shown previously (29) to bind to Tax in a two-hybrid system. TXBP151 is a novel A20-binding protein, which mediates the anti-apoptotic activity of A20, and its overexpression inhibits apoptosis induced by TNF or CD95 (Fas/APO-1) (29).

To simplify the data base search process, analysis of each spot was limited to the best one protein match in the data base. However, it appeared that some spots were contaminated with other minor proteins, which could not be separated with chromatography or 2-D gels. For instance, spots 1, 2, and 3 appeared as modifications of a protein with varying pI and slight alterations in molecular mass (Fig. 2*A*). However, the MS analysis suggested that they may contain two proteins, *e.g.* gelsolin, which was the first protein identified in the data base search for spots 2 and 3, and ras GAP^{1m}, which ranked as the first candidate for spot 1.

We then confirmed some of the Tax-binding proteins from Table II using immunoprecipitation followed by Western blot analysis. Those proteins, which were mainly related to small GTPase-skeletal dynamics and nucleosome remodeling (SWI/SNF), were chosen for further study. The GTPases regulate many cytoplasmic signaling pathways, and SWI/SNF is a nuclear chromatin remodeling complex. Interestingly, a direct link between SWI/SNF and RhoA signaling pathway has been shown to allow formation of actin stress-fiber-like structures (59). When immunoprecipitated complexes were washed under low salt wash conditions (150 mM), all of the selected proteins from Table II showed positive associations with Tax (Fig. 3*A*). However, only a handful of these proteins, namely GAP^{1m}, Cdc42, and actin, could withstand washes with the high salt wash buffer (1000 mM; see Fig. 3*B*). Further confirmation was performed using immunoprecipitation with anti-Tax and Western blot with various antibodies. Fig. 3*C* also shows that Tax is

TABLE I
A list of matched peptide sequences in Fig. 2D

Spot no.	Measured mass	Computed mass	Residues			Matched peptide sequence
			Start	To	Cut	
1	995.528	995.576	358	366	0	NDAVLPLVR
	1012.524	1012.577	110	117	1	NVLQRDLR
	1150.682	1150.649	49	58	0	NLLPYLGPHK
	1723.794	1723.79	775	790	0	MEEACGTIAVYQGPQK
	2362.142	2362.183	336	357	1	SPDVQPISASAAYILSEICRDK
	2478.137	2478.312	274	294	1	VPVNVLRTDSSHQAWYLLQPR
	2770.313	2770.319	463	486	1	LFNTIVKSSMSCPTVMCDIFYSLR
2	1077.482	1077.509	730	738	0	YIETDPANR
	1274.701	1274.709	178	188	0	HVVPNEVVVQR
	1318.68	1318.688	585	597	0	AGALNSNDAFVLK
	1348.628	1348.637	730	740	1	YIETDPANRDR
	1665.005	1664.773	714	728	1	DSQEEEKTEALTSAK
	2047.134	2047.062	531	548	0	EPAHLMSLFGGKPMIIYK
	2063.096	2063.057	531	548	0	EPAHLMSLFGGKPMIIYK
	2314.208	2313.153	143	162	1	AVQHREVQGFESATFLGYFK
	2462.298	2462.21	303	327	0	VSNGAGTMSVSLVADENPFAQGALK
	2478.252	2478.205	303	327	0	VSNGAGTMSVSLVADENPFAQGALK
	2770.461	2770.327	458	481	0	VPVDPATYGQFYGGDSYIILYNYR
	2872.454	2872.274	420	447	0	VPFDAATLHTSTAMAAQHGMDDDGTGQK
	2904.437	2904.264	420	447	0	VPFDAATLHTSTAMAAQHGMDDDGTGQK
4	1036.528	1036.518	152	161	1	YGKAGSPETK
	1200.643	1200.609	390	399	1	RLQAEAEEQK
	1275.638	1275.552	251	259	0	WVWDQEEER
	1364.707	1364.62	434	446	0	TEEASSGFLPGDR
	1372.678	1372.599	451	462	0	STTELDDYSTNK
	1382.708	1382.679	640	651	1	RICSYCNNILGK
	1474.79	1474.726	1	13	1	QKEVAATEEDVTR
	2223.078	2223.007	321	340	1	EPSLATWEATWSEGSKSSDR
	2467.236	2467.137	34	57	0	ATLSSTSGLDLMSESGEGEISPQR
6	1125.589	1125.56	132	141	1	NLVYSCRGSK
	1527.77	1527.771	29	42	0	MQIVTALDHSTQGK
	1543.767	1543.766	29	42	0	MQIVTALDHSTQGK
	1673.831	1673.771	576	590	0	MEPADYNSQIIGHSL
	1712.841	1712.797	275	290	0	DLSHCGGDMPVVQSLR
	3142.507	3142.548	220	249	1	SAGLLDSGMFVNIHPSGIKTEPAMLMAPDK
	3158.452	3158.543	220	249	1	SAGLLDSGMFVNIHPSGIKTEPAMLMAPDK
7	976.474	976.465	354	360	0	FLYEYSR
	1291.71	1291.702	570	581	0	TVVGEFTALLDK
	1310.753	1310.734	362	372	0	HPDYSVVLLLR
	1466.855	1466.835	361	372	1	RHPDYSVVLLLR
	1471.761	1471.724	157	168	0	AFFGHYLYEVAR
	1524.847	1524.85	439	452	0	VPQVSTPTLVEISR
	1527.784	1527.781	397	409	0	VLDEFQPLVDEPK
	1652.954	1652.945	438	452	1	KVPQVSTPTLVEISR
	1901.935	1901.934	170	184	0	HPYFYAPELLYYAQK
	2058.054	2058.036	169	184	1	RHPYFYAPELLYYAQK
	2314.075	2314.08	150	168	1	AFHDDEKAFFGHYLYEVAR
16	1050.557	1050.534	314	324	0	AASAYAVGDVK
	1130.734	1130.636	237	246	1	MKIVDVIGEK
	1192.543	1192.565	336	345	0	LLGPCMDIMK
	1244.492	1244.635	250	260	1	DGERIITQGEK
	1364.586	1364.661	336	346	1	LLGPCMDIMKR
	1366.633	1366.637	325	335	0	CLVMDVQAFER
	1382.615	1382.632	325	335	0	CLVMDVQAFER
	1405.592	1405.654	358	370	0	MFGSNLDLLDPGQ
	2468.178	2468.174	325	345	1	CLVMDVQAFERLLGPCMDIMK
19	1117.47	1117.653	267	276	0	VVYIFGPPVK
	1140.494	1140.638	110	119	1	EEGKVIEPLK
	1192.633	1192.543	232	242	0	SYSYVCGISSK
	1328.649	1328.698	335	345	1	QPSCQRSVVIR
	1380.667	1380.641	154	164	0	VICAEEPYICK
	1765.837	1765.954	315	329	0	ISQMPVILTPLHIFDR
	2363.393	2363.266	315	334	1	ISQMPVILTPLHFDRDPLQK
25	867.441	867.376	126	131	0	MICICR
	1050.587	1050.513	126	134	1	MICICRNAK
	1178.511	1178.561	71	79	1	CRQDAIFNR
	1333.574	1333.662	189	198	0	ILFIFYEDMK
	1790.73	1790.982	108	122	1	THLPPRLLPASFWEK
	2580.294	2580.264	28	49	0	YWDNVEAFQARPDDLVIAAYPK

able to associate with Cdc42, gelsolin, Rad51, GAP^{1m}, and cdk2 when performing reverse immunoprecipitations. Cdc42, GAP^{1m}, and actin are functionally related to the small GTPase superfamily and involved in cytoskeletal organization (30, 31). Finally, to confirm a possible interaction between Tax and the SWI/SNF complex, immunoprecipitations using anti-BAF53, -BAF57, -BAF155, and -BRG1 antibodies were performed, and bound complexes were washed in high salt, followed by Western blots with anti-Tax antibody (Fig. 3*D*). Reverse immunoprecipitation with anti-Tax and Western blotting against BAFs

TABLE II
Tax-binding protein candidates identified by MALDI-TOF-MS analysis

Spot no.	Name	NCBI ID no.	PI	MM	Coverage	Peptide matched
				kDa	%	
1	Ras P21 proactivator 2 (GAP^{1m})	5730003	6.7	97.13	12	7
2	Gelsolin	4504165	5.9	85.68	19	13
3	Gelsolin	2833344	5.6	80.81	13	7
4	KIAA0858 protein [LIM domain]	4240205	5.5	80.33	17	9
5	Tax 1-binding protein 1	11421738	5.7	68.44	16	7
6	Nuclear receptor subfamily 2	6755861	6.3	65.51	14	7
7	Serum albumin precursor	1351909	5.8	68.90	15	11
8	Serum albumin precursor	1351909	5.8	68.90	15	11
9	Cdc42/Rac effector kinase; PAK-3	3420949	5.3	60.75	14	7
10	Myosin light chain kinase (MLCK)	125494	5.0	65.80	8	5
11	Putative phenylalanine-tRNA synthetase	13877969	6.0	49.23	28	8
12	Cytochrome P450 2D28 (CYPIID28)	10719966	7.3	56.55	14	5
13	Recombination activator protein 2	12247641	5.1	50.11	17	8
14	DJ710L4.2 (similar to myotubularin-related protein)	4490506	6.3	45.59	25	9
15	H-2 class I histocompatiblity antigen (h-2kb)	122142	6.0	41.28	22	7
16	Protein kinase, cAMP-dependent, type II, α	4758958	5.0	45.50	16	9
17	Stimulated trans-acting factor (50 kDa)	5174699	7.1	50.44	23	10
18	SWI/SNF (BAF 57)	065643	6.2	53.24	19	8
19	Guanine monphosphate synthetase	11432448	6.4	44.77	18	7
20	MHC class I Patr-B*06	1255180	5.4	39.33	25	5
21	Annexin 14	6274497	5.2	37.09	20	5
22	Urokinase plasminogen activator receptor	11875701	5.9	36.65	34	8
23	Actin prepeptide	178067	5.2	36.79	25	4
24	44-kDa protein kinase	1335009	6.3	40.98	23	7
25	Estrogen sulfotransferase	1711603	6.7	35.23	24	6
26	RAD51 (*S. cerevisiae*)-like 1	12738562	6.7	40.40	18	7
27	Apoptosis inhibitory 6, Sp-α	6753092	5.1	38.89	22	6
28	AMBP protein precursor	2507586	5.7	37.67	34	6
29	BM-017	7582306	6.0	38.38	14	4
30	Tropomyosin 5	9653293	4.7	28.93	20	6
31	Actin	7546746	5.5	24.53	35	5
32	Putative Orf (AK006023)	12838908	5.7	25.14	17	4
33	Tumor protein D52-like 2; hD54	4507643	5.3	22.19	14	3

and BRG1 were also performed (Fig. 3*E*). The results demonstrated that at least four components of the SWI/SNF complex, namely BAFs 53, 57, and 155, and BRG1, were detected in the Tax immunoprecipitates. Collectively, these data imply that Tax interacts with multiple cytoplasmic and nuclear proteins, which may contribute to the ability of Tax to control signal transduction and transcription of many cellular genes.

Cytoplasmic Tax Interacts with Small GTPases—The Ras p21 proactivator 2 (GAP^{1m}) (spot 1) and Cdc 42/Rac effector kinase PAK-3 (spot 9) (see Tables I and II) bind and regulate RhoA, Rac1, and Cdc42, all of which are cytoplasmic small GTPase proteins. We, therefore, focused on these particular small GTPase superfamily members (*i.e.* Cdc42, RhoA, and Rac1). Tax binding was assessed by a pull-down assay with GST fusion proteins and Western blotting with anti-Tax antibody. Fig. 4*A* demonstrates that Tax from C81 cells could bind to the GST-Cdc42, -RhoA, and -Rac1 fusion proteins. Furthermore, GST-Tax could also bind to the Cdc42 protein from both infected and uninfected cell lysates (Fig. 4*B*). Interestingly, the binding of Tax to Cdc42 was promoted by a factor(s) from cell lysates when compared with binding of the purified Tax to GST-Cdc42 (Fig. 4*C*, *lane 4*). To address whether the binding of purified Tax to Cdc42 was specific and not as a result of an increase in total protein from CEM cells, we incubated a fixed amount of Tax and GST-Cdc42 with increasing amounts of CEM lysate (*lane 6*, 200 ng; *lane 7*, 500 ng; and *lane 8*, 1000 ng). As seen in Fig. 4*B*, *lanes 6–8*, increasing amounts of CEM extract did not result in an increase in the amount of Tax binding to GST-Cdc42.

Small GTPases are turned on and off by binding to GTP/GDP nucleotides *in vivo*. However, from our current experiments, it was not clear whether binding of Tax to Cdc42 was independent of, or resulted from, association with nucleotides present in the cell extracts. This was further tested through mixtures of reaction components as shown in Fig. 4*D*. When assaying for Tax binding from the C81 lysate with various nucleotides, it was found that GTP, and not GDP, activated Tax binding to Cdc42. Various concentrations of GTPγs and GDPβs (0.1, 0.5, and 1 μM) were incubated with a fixed amount of C81 extract and pulled down with GST-Cdc42. Results in Fig. 4*D* provide compelling evidence that Tax binds to the active form of small GTPase, such as Cdc42, RhoA, and Rac1, and may modulate cytoplasmic second messengers.

Tax Interacts with Transcription/Chromatin Remodeling Factors—To assess whether the interaction of Tax with SWI/SNF was indeed functional, we designed an *in vitro* ChIP assay using Tax targeted to the polymerase II transcription machinery (32). SWI/SNF complexes are present in cells in multiple forms composed of 9–12 proteins that are referred to as BAFs ranging from 47 to 250 kDa. We used a purified system to analyze the function of SWI/SNF in site-specific chromatin remodeling, as well as its distribution, function, and retention following recruitment by Tax. To analyze the binding of SWI/SNF to the template, we performed an *in vitro* ChIP assay from micrococcal nuclease-digested nucleosomal templates in the presence or absence of competitor chromatin (32). To ensure the presence of a chromatin structure in our salt reconstitution assays, we first used micrococcal nuclease digestion of plasmid pG5E4T DNA (five Gal4 binding sites upstream of the adenovirus 2 E4 minimal promoter) following *in vitro* reconstitution. Chromatin was analyzed by digesting plasmid DNA at each time point with micrococcal nuclease at room temperature. Reactions were stopped, proteins were digested with proteinase K, and following DNA precipitation, samples were run on a 1.2% agarose gel. Results in Fig. 5*A* indicated that we were able to reconstitute the pG5E4T DNA into nucleosomal arrays *in vitro*. Subsequently, we performed ChIP assays from digested nucleosomal templates in the presence or absence of competitor

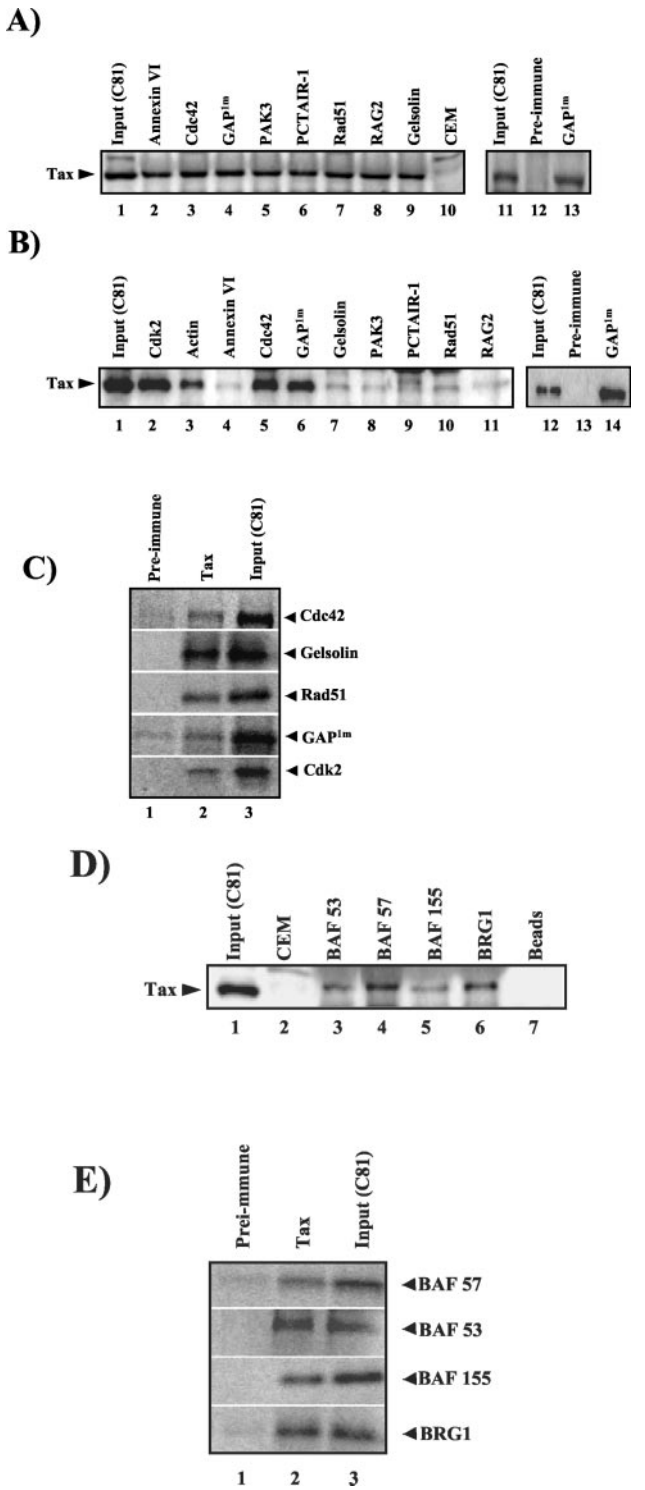

FIG. 3. **Immunoprecipitation followed by Western blotting using antibodies against suggested protein candidates from Table II.** Immunoprecipitations were performed with 2 mg of total cellular protein and 10 μg of antibody. After immunoprecipitation with various antibodies, protein A/G beads were added and complexes were washed with a low salt (*panel A*, 150 mM NaCl in TNE; see "Experimental Procedures") or high salt (*panels B–E*, 1000 mM NaCl in TNE) wash solution. Control immunoprecipitations consisted of pre-immune antibody (IgG purified, *panels A* and *B*, *lanes 12* and *13*, respectively) and pre-immune sera (IgG purified, *panels C* and *E*, *lanes 1*). *Panels A*, *B*, and *D* are immunoprecipitations with various antibodies and Western blotted with anti-Tax antibody. *Panels C* and *E* are immunoprecipitations with anti-Tax antibody and Western blotted with various antibodies. Following separation on 4–20% SDS-PAGE, the target protein bands were detected with specific antibodies (10 μg/10 ml of TNE 50) as indicated (*arrow*). *Input lanes* represent [1/50] of the extract used for immunoprecipitations.

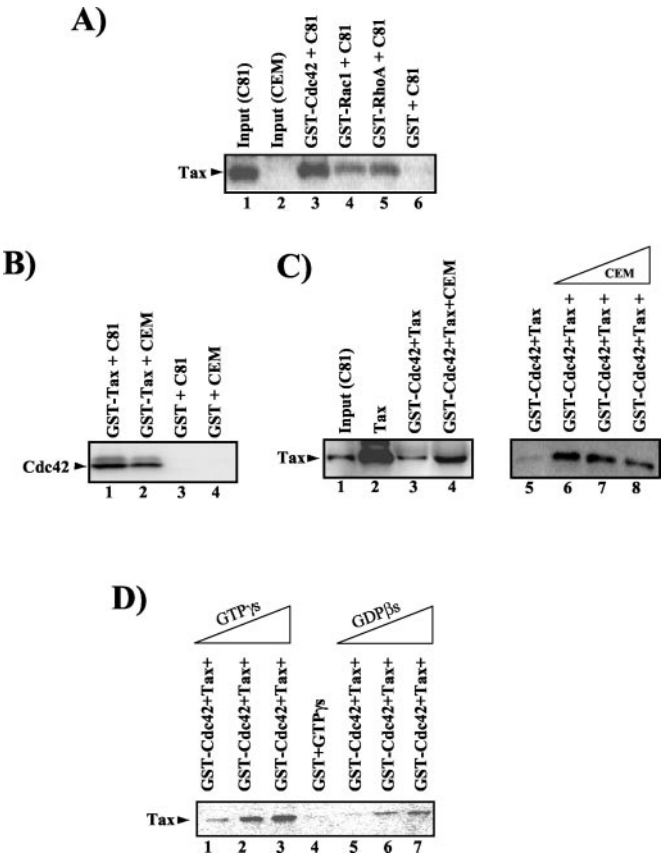

FIG. 4. **Pull-down assays for detection of Tax binding to small GTPases.** *A*, 2 μg of purified GST-Cdc42 (*lane 3*), GST-Rac1 (*lane 4*), GST-RhoA (*lane 5*), and GST (*lane 6*) were incubated with 1 mg of C81 lysate, pulled down with glutathione-Sepharose beads, washed, and run on 4–20% SDS-PAGE, and Western blotted with anti-Tax polyclonal antibody. *B*, GST-Tax protein-Sepharose beads were mixed with C81 or CEM lysates, bound, and washed, and bound Cdc42 was identified with anti-Cdc42 antibody (*lanes 1–4*). GST-Sepharose beads were used as a control. *C*, purified Tax protein from *E. coli* (1 μg) was used in a pull-down assay with GST-Cdc42 protein beads in the absence (*lane 3*) or presence (*lane 4*) of CEM lysate (200 ng). To address whether the binding of purified Tax to Cdc42 was specific and not as a result of increase in total protein from CEM, a constant amount of Tax and GST-Cdc42 were incubated with increasing amounts of CEM lysate (*lane 6*, 200 ng; *lane 7*, 500 ng; and *lane 8*, 1000 ng). *D*, role of GTPγs and GDPβs in the binding of Tax to Cdc42. Various concentrations of GTPγs and GDPβs (0.1, 0.5, and 1 μM) were incubated with a constant amount of C81 extract and pulled down with GST-Cdc42. *Lanes 1* and *5* contained 0.1 μM, *lanes 2* and *6* contained 0.5 μM, and *lanes 3* and *7* contained 1 μM of exogenously added nucleotides. *Lane 4* serves as negative control with GST alone. All samples were further incubated overnight at 4 °C. Reaction volumes were 200 μl in total. Samples were washed the next day with TNE_{1000} and 0.1% Nonidet P-40, run on a gel, and Western blotted for the presence of Tax protein.

chromatin. After cross-linking and washing, the pG5E4T nucleosomal array templates were digested with MNase. The fragmented material was then immunoprecipitated using affinity matrix HA antibody against an HA tag available on the hSwi2/Snf2 subunit (33). Following reversal of the cross-links, the DNA, which was associated with the immunoprecipitated hSWI/SNF complex, was purified, slot blotted, and probed with full-length pG5E4T plasmid and probes to various locations on the plasmid. The positions of the different probes used for these ChIP studies are shown in Fig. 5*B*. We used Gal4 alone, Gal4-VP16, Gal4-Tax (WT), and Gal4-Tax (M47) as a source of activator proteins in these assays. When Gal4-VP16 (positive control) and Gal4-Tax were bound to the array, the fragments that were closest to the Gal4 binding sites were preferentially immunoprecipitated, indicating that both activators recruited

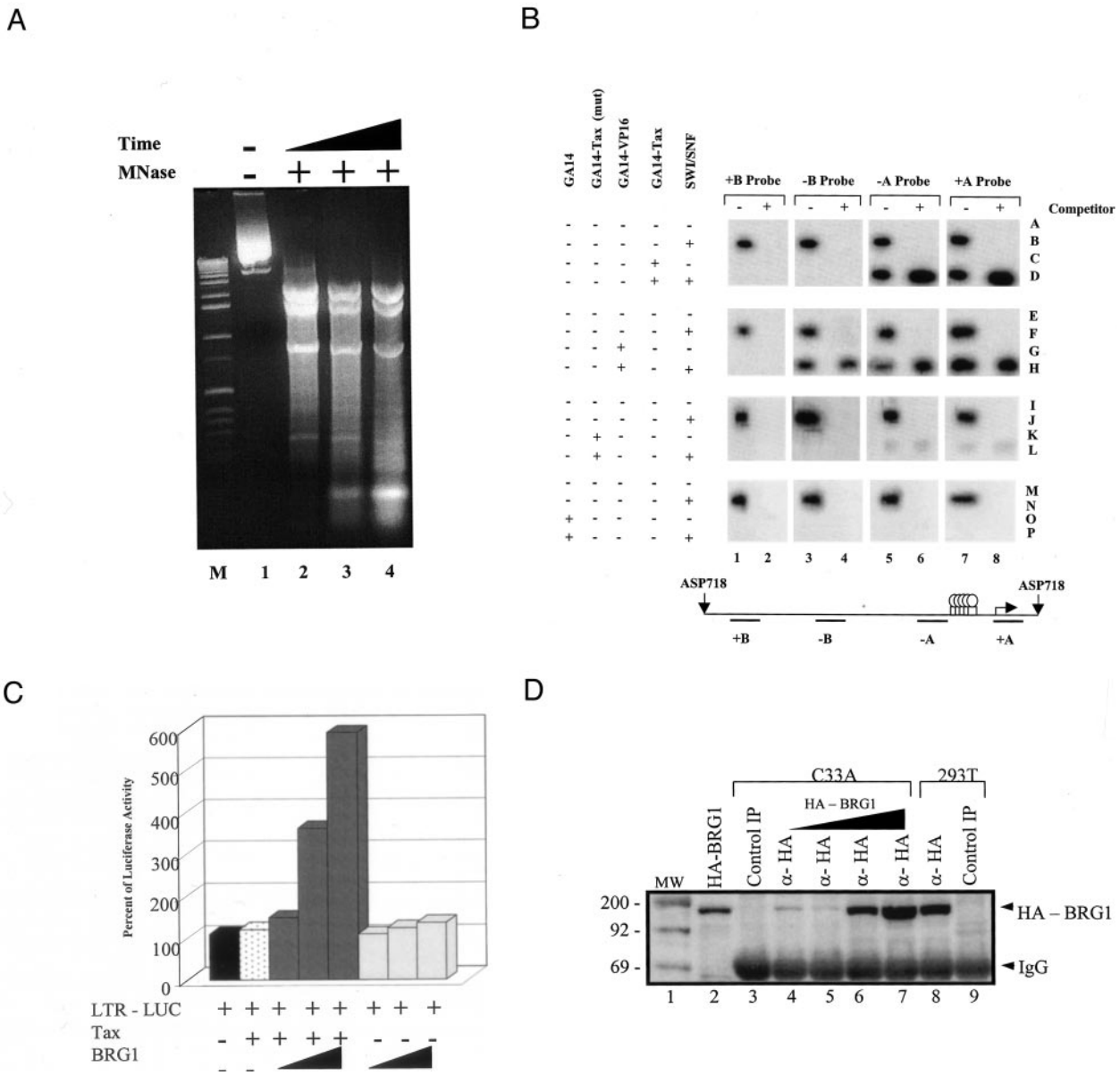

FIG. 5. **Functional interaction of Tax with the chromatin remodeling complex.** *A*, micrococcal digestion of pG5E4T chromatin template. Chromatin was digested with micrococcal nuclease for 0 min (*lane 1*), 0.5 min (*lane 2*), 1 min (*lane 3*), or 5 min (*lane 4*). DNA was purified and analyzed on a 1.2% agarose gel. *B*, biotinylated pG5E4T nucleosomal arrays were bound to paramagnetic beads coupled to streptavidin and incubated in the presence or absence of Gal4, Gal4-Tax (WT), Gal4-Tax (M47 mutant), and/or Gal4-VP16, followed by the addition of SWI/SNF and competitor chromatin. After cross-linking and washing, the templates were digested with MNase and immunoprecipitated using affinity matrix HA antibody to pull down SWI/SNF (the Swi2/Snf2 subunit was HA-tagged). DNA from the precipitates was slot blotted and probed with the DNA fragments indicated *above* the blot (+*B*, −*B*, −*A*, and +*A*). Positions of the different probes when pG5E4T was digested with Asp-718 are shown at the *bottom*. *C*, transfection of BRG1 with HTLV-1 LTR in C33A (*BRG1 mutant*) cells. pLTR-luciferase (*LTR-LUC*; 10 μg), pCMV-Tax (*Tax*; 3 μg), and pHA BRG1 (0.1, 1, and 3 μg) were transfected into C33A cells, harvested 24 h later, and assayed for the presence of the luciferase enzyme. *D*, pHA-BRG1 (0.1 μg, *lane 4*; 0.5 μg, *lane 5*; 1 μg, *lane 6*; and 3 μg, *lane 7*) was transfected into C33A cells, immunoprecipitated with 12CA5 monoclonal antibody, washed, run on a 4–20% SDS-PAGE, and Western blotted with an anti-BRG1 antibody. *Lane 2* is 300 ng of purified HA-BRG1 eluted from a 12CA5 column with 40-fold excess HA-peptide (positive control for Western blot). *Lane 3* is a negative control (mock transfection in C33A cells) with no plasmid and immunoprecipitations with HA-antibody. *Lane 8* is a positive control for transfection of pHA-BRG1 (3 μg) into 293 cells, followed by immunoprecipitations with HA antibody. *Lane 9* is a negative control (mock transfection in 293 cells) with no plasmid and immunoprecipitations with HA antibody. *E*, presence of acetylated histone H4 on HTLV-1 DNA. C33 cells were transfected with HTLV-I-LTR-CAT (10 μg), Tax (3 μg), and/or HA-BRG1 (3 μg). Total DNA was obtained 48 h post-transfection for a ChIP assay. *Lanes 1–4* serve as input controls prior to immunoprecipitation with anti-histone H4 (Lys-16) antibody. *Lanes 5–7* represent control IgG antibody (5 μg) for ChIP analysis. *Lanes 8–10* represent ChIP with anti-H4 (Lys-16)-specific antibody (5 μg). The recovered DNA was used amplify to the LTR region (U3/R) from the HTLV-I promoter. The sequence of the 5′ and 3′ primers (20-mer) were at −300 (areas upstream of ETS, TRE1, and TRE2 sites) and the 5′ primer from +150. The resulting U3/R PCR product was 450 bases. *F*, suppression of BRG1 expression by RNAi inhibits HTLV-1 replication. HTLV-1-infected cells (*C91/PL* and *MT-2*) were treated with TNF-α (10 ng/ml) for 2 h, washed, and subsequently electroporated with increasing amounts (1, 5, or 10 μg) of either WT or mutant (*mut*) BRG1 siRNA. Seven days later, samples were collected and used for p19/gag enzyme-linked immunosorbent assay. *G*, suppression of BRG1 by RNAi inhibits HTLV-1 LTR promoter activity. HTLV-1-infected cells (*C91/PL* and *MT-2*) were treated with TNF-α (10 ng/ml) for 2 h, washed, and subsequently electroporated with increasing amounts (1, 5, or 10 μg) of either WT or mutant (*mut*) BRG1 siRNA. Twenty-four h later, nuclear RNA were collected and used for reverse transcriptase PCR. Reverse transcription was performed with 1 μg of nuclear RNA with a primer (30-mer) at position +300. The sequence of the 5′ and 3′ primers (20-mer) for PCR were at position +1 (5′ primer), and position +150 (3′ primer). The resulting R region PCR product was 150 bases. We consistently saw two bands in MT-2 cells, because these cells contain eight copies of viral DNA, two of which are integrated infectious clones, and one integrated copy that is missing 14 nucleotides at position +80 to +94 (F. Kashanchi, unpublished results).

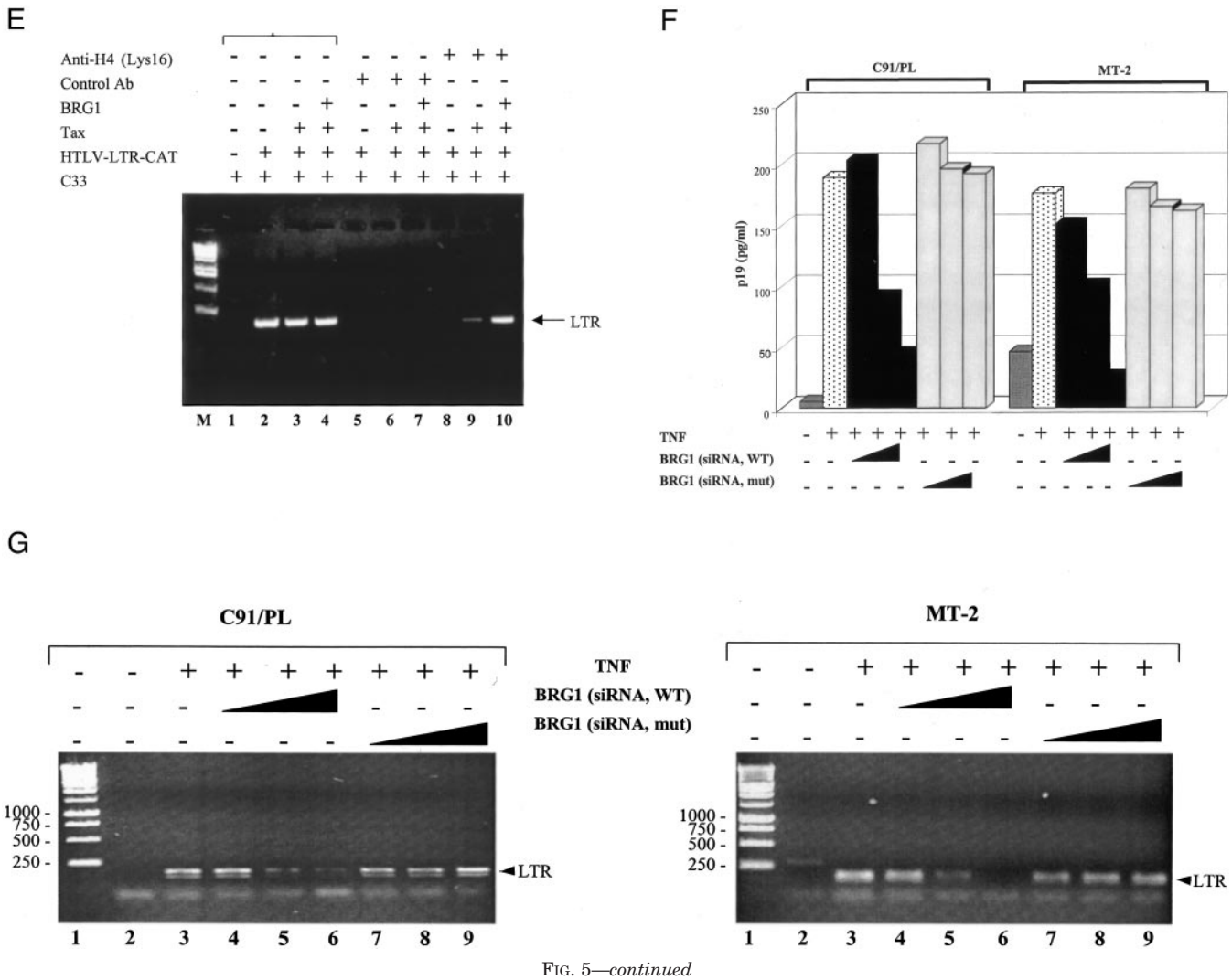

FIG. 5—*continued*

SWI/SNF to the template nucleosome array and localized the complex to the promoter or nearby sequences. Interestingly, unlike VP-16, Tax recruitment of SWI/SNF was limited and localized to an area adjacent to the GAL4 DNA binding sites (Fig. 5*B*).

To verify that Tax association with BRG1 results in activation of HTLV-1 LTR expression, co-transfections were performed in C33A cells, which express a mutant form of BRG1. HTLV-1 LTR luciferase was transfected with Tax and BRG1 into C33A cells. Increasing amounts of luciferase was observed when Tax was transfected with increasing amounts of BRG1 (Fig. 5*C*). Transfecting increasing amounts of BRG1 resulted in higher levels of expression as determined by Western analysis (Fig. 5*D*). Therefore, induction of HTLV-1 LTR expression by Tax required BRG1 protein. An *in vivo* ChIP assay was used to show that co-expression of Tax and BRG1 in C33 cells resulted in acetylation of histone H4 on the HTLV-1 promoter (Fig. 5*E*). These results indicate that Tax recruits BRG1 to the HTLV-1 promoter and induces acetylation of histone H4, thereby activating HTLV-1 LTR expression.

Tax recruitment of SWI/SNF to the HTLV-1 LTR presumably plays a role in the ability of Tax to transactivate the promoter and induce replication. To assess this possibility, RNA interference of BRG1 expression in HTLV-1-infected cells was used. Double-stranded RNA induces gene-specific silencing in organisms from fungi to animals, a phenomenon known as RNA interference (RNAi). RNAi represents an evolutionarily conserved system to protect against aberrant expression of genes and a powerful tool for gene manipulation. It has been shown recently in cultured mammalian cells that siRNAs of 21–23 nucleotides can mediate RNAi, resulting in specific degradation of a given mRNA thereby allowing a loss-of-function phenotype. Therefore, to define the functional significance of Tax/BRG1 in infected cells, we synthesized a series of wild type and mutant siRNA against BRG-1. Oligos were designed and synthesized using the OligoEngine website at www.oligoengine.com. We entered the accession number for BRG1 from PubMed and created many candidate siRNAs. We chose five oligos that span the 5′ end, middle, and 3′ end of the BRG1 mRNA. The sequences of the siRNA and the nucleotide position are listed under "Experimental Procedures." Replication was induced in the HTLV-1-infected cell lines C91/PL and MT-2 by treatment with TNF-α (Fig. 5*F*). Electroporation of increasing amounts of wild type BRG1 siRNA (a mixture of all five oligos) resulted in a decrease in p19/gag antigen expression. However, when mutant BRG1 siRNA was used, p19/gag expression and, hence, HTLV-1 replication, was unaffected. Finally, to ensure that the increased in p19/gag levels (free virion in supernatants) were the result of increased viral promoter (LTR) transcription, we performed reverse transcriptase PCR from C91/PL and MT-2 cells treated with wild type and mutant BRG1 siRNAs. Results of such an experiment are shown in Fig. 5*G*, where wild type and not the mutant siRNA reduced viral transcription in both cell types. Collectively, these results in-

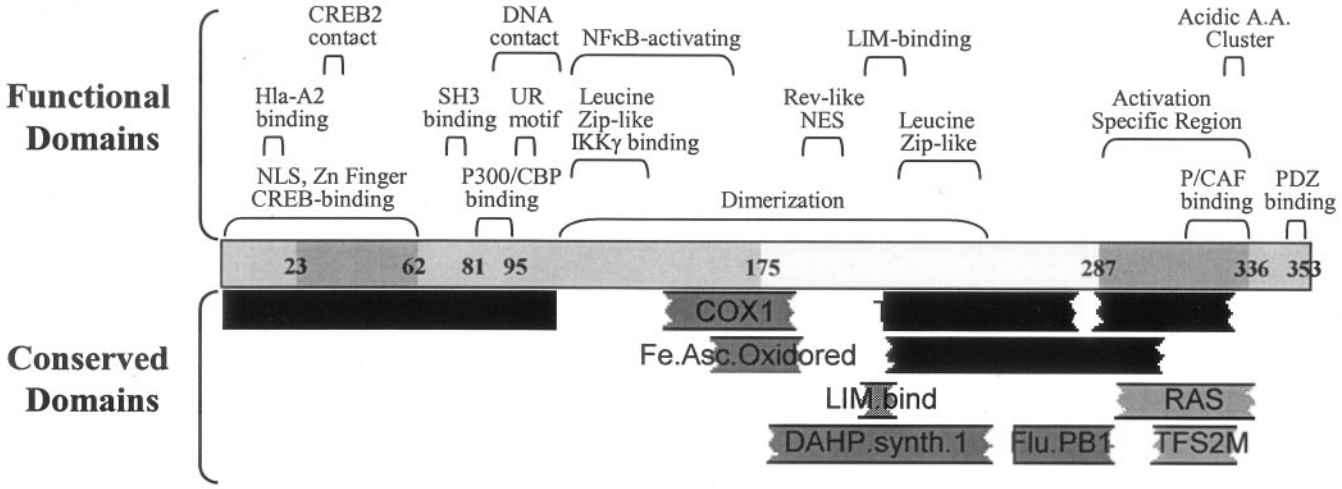

FIG. 6. **Schematic display of structural and functional regions of the Tax protein.** The Tax (NCBI accession number 6983837) protein schematic is modified from the "conserved domain search" in BLAST (www.ncbi.nlm.nih.gov/BLAST/) with the E value at 10. Each domain with its score (1st data *in parentheses*) and E value (2nd data) were as follows: *Tax* (166, 2e-42); *transpeptidase* (31.2, 0.099); *hemagglutinin* (30.0, 0.22); *ras/Ras family* (29.3, 0.38); *RAS/RAS small GTPases* (26.2, 3.2); *COX1* (25.4, 5.4); *TFS2M* (25.4, 5.4); *Flu_PB1* (25.0, 7.1); *Fe_Asc_oxidored* (25.0, 7.1); *LIM domain-binding protein* (24.6, 9.3); *DAHP synthetase I family* (24.6, 9.3). *Above* the scheme is a display of the possible functional and structural regions of Tax according to various websites (pbil.univ-lyon1.fr/pbil.html, pfam.wustl.edu) and literature searches. *UR*, upstream region (14); *NES*, nuclear export signal (2); *NLS*, nuclear localization signal.

dicate that BRG1 expression is critical for activated transcription and HTLV-1 replication.

DISCUSSION

We have used chromatography, immunoaffinity purification, 2-D gel electrophoresis, and MALDI-TOF analysis to identify cellular proteins that interact with Tax in HTLV-1-infected cells. The Tax-containing 1800-kDa fraction was analyzed and was found to contain cellular proteins involved in signal transduction, the cytoskeleton, and transcription/chromatin remodeling. A few of these proteins have been shown previously to bind to Tax in a two-hybrid system, including TXBP151.

Tax bound to several small GTPase proteins, including ras GAP^{1m}, Rac1, Cdc42, RhoA, and gelsolin. Small GTPases function by partnering with the cytoskeletal proteins. Small GTPases could regulate more than 10 proteins listed in Table II. Consistent with this notion, Tax may also communicate with the JNK pathway, because JNK components are largely regulated by small GTPases. Previous experiments have demonstrated that constitutive activation of JNK promotes interleukin-2-independent growth in HTLV-1-infected T-cells (18, 34). Thus, an indirect activation by Tax may affect many JNK downstream targets including DNA-binding transcription factors and MEKKs. For instance, Yin *et al.* (35) have shown that Tax associates with and activates MEKK1 when the two proteins are over-expressed *in vivo*. Furthermore, these two activities were lost when Tax was mutated at sites that required activation of IKK and NFκB. However, our results, based on physical protein-protein interactions, imply that Tax modulates the upstream effector proteins in combination with small GTPases, which in turn control downstream signaling cascades, such as JNK, p38, MEKKs, and NFκB complexes (1, 36). Consistent with our findings, Jin *et al.* (18) have found that a novel upstream protein, G-protein pathway suppressor 2, physically interacts with Tax and modulates activation of the JNK pathway.

Previous studies have also shown that Tax binds to α-internexin (37), a neuronal intermediate filament protein, and cytokeratin (38) to regulate the networks of vimentin and cytokeratin (39, 40). The Tax binding site in α-internexin is at the central rod region (coil 1), which is required for the formation of a coiled-coil dimer, the first step in intermediate filament assembly. The same structure is required for Tax to bind keratin 8 (38). The domain of Tax involved in binding is separable from those domains involved in transactivation (37, 38). Several of our identified component proteins belong to cytoskeletal protein families, including gelsolin and actin, and/or are related to cytoskeletal dynamics, *e.g.* annexin, myosin light chain kinase, and myotubularin-related protein (dJ710L4.2; see Table II). Small GTPases, including Cdc42, RhoA, and Rac1, are also best known for their effects on the actin cytoskeleton leading to transformation (31, 41, 42). For example, in fibroblasts, activation of Cdc42 causes the formation of filopodia, activation of Rac results in the formation of lamellipodia and membrane ruffling, and activation of Rho leads to the formation of stress fibers (41–44). Furthermore, there are at least six known substrates of Rho-associated kinases, which play a critical role in actin cytoskeletal reorganization (41), three of which are related to Rho-associated kinase function (a LIM-containing domain (spot 4), an ERM domain (spot 5), and a MLC domain (spot 10)), that are present in the Tax-binding protein complexes (Table II).

In human cells, homologs of the yeast SWI2/SNF2 protein (BRG1 and hBRM) are implicated in chromatin remodeling, as well as activation and growth control. *In vitro*, the packaging of DNA into chromatin prevents access of DNA binding factors and inhibits elongation by RNA polymerase II. Indeed, the activation of many genes is accompanied by a disruption of the pattern of nucleosomes over promoters and transcribed regions. Consistent with the current view of SWI/SNF recruitment of site-specific activators, we also found that the Tax/SWI/SNF binding may be recruited to an active promoter (Fig. 5*B*). In addition, two different classes of chromatin remodelers may function at separate and successive steps in gene activation. Therefore, according to our previous results and those of others with Tax/CBP interactions, we suspect that, much like the HO promoter in yeast, there may be a cell cycle-regulated wave of SWI/SNF-dependent histone modification that is restricted to ~1 kb of the Tax responsive viral and cellular promoters (including the HTLV-1 promoter elements upstream of the TATA box and the cyclin D2 promoter) (45). Future experiments using *in vivo* ChIP assays will determine whether histone H3 and H4 acetylation at the HTLV-1 and cyclin D2

promoters do indeed occur at the G_1 phase of the cell cycle.

Tax Structural Bioinformatics—Based on reported studies and our bioinformatic analysis, the specific functional and structural regions of Tax are shown in Fig. 6. The figure defines known modules in Tax and its similarities with other protein domains and attempts to explain the multifunctional activities of Tax, which rely mainly on protein-protein interactions. The lower half of the schematic identifies conserved domains of the Tax polypeptide (Entrez/accession number 6983837).

The upper half of the scheme lists functional regions of the Tax protein. They include binding regions to CREB, p300/CBP, NFκB, and others from previously published results (1, 3, 14, 15, 17). There are two leucine zipper-like (*Leucine Zip-like*) regions (sequences 116–145 and 213–248) in Tax, both of which are missing one leucine when compared with a typical leucine zipper motif (L*X*(6)L*X*(6)L*X*(6)L). The total length of these regions is larger than a typical leucine zipper and is involved in protein dimer formation (14, 46). There is a PDZ binding motif at the C-terminal region of Tax with an *XTXV* consensus sequence. This region is involved in the interaction of Tax with six proteins containing a PDZ domain (47). PDZ domains play critical roles in interaction with the cytoskeleton, in the organization of the Rho pathway (both upstream and downstream), and in scaffolding (48, 49). Amino acids 106 to 111 of Tax encompass a conserved region with a predicted α-helix and may function as an interaction surface with IKKγ (14). Two other possible active domains in Tax are an SH3 binding region (amino acids 73–79) and a LIM binding domain (amino acids 207–219), both of which are critical for protein-protein interactions. Interestingly, spot 4 (see Fig. 2 and Table II) has a LIM domain, as well as a PDZ domain. LIM domains are cysteine-rich domains composed of two special zinc fingers that are joined by a two-amino acid spacer. LIM proteins form a diverse group, which includes transcription factors and cytoskeletal proteins. LIM-only proteins are also implicated in the control of cell proliferation, because several genes encoding such proteins are associated with oncogenic chromosome translocation (50). LIM-only proteins, such as ACT, specifically associate with cAMP response element modulation and CREB and stimulate transcriptional activity in yeast and mammalian cells in the absence of the classical CBP/p300 pathway (51, 52). Therefore, it is possible that the LIM-containing protein (spot 4) binds Tax at either amino acids 207–219 or amino acids 22–53 (which has a Zn-finger domain) and controls transcriptional activation (53).

It has been reported that Tax can bind to its partners through a coiled-coil structure (19). Therefore, we scanned all the proteins from Table II using coiled-coil prediction software (PBIL, pbil.univ-lyon1.fr/pbil.html) and found that there were at least eight proteins (spots 1, 3, 5, 11, 17, 25, 26, and 33; see Fig. 2 and Table II) that contain coiled-coil structures. There are also more than 10 proteins in Table II that are structurally and/or functionally related to cytoskeletal dynamics (spots 1, 2, 3, 5, 9, 10, 14, 21, 23, and 31). Among those related proteins, gelsolin (spots 2 and 3) is an essential downstream effector of Rac-mediated actin dynamics (54).

Tax1-binding protein (spot 5) also contains a coiled-coil region and ERM and myosin tail-like domains ($E \ll 0.01$; BLAST). A TRAF-interacting protein, T6BP, which is almost identical to TXBP151, specifically associates with TRAF6 through an N-terminal ring and zinc-finger domains (55). Spot 14, which contains a protein-tyrosine phosphatase motif, is a myotubularin-related protein. Myotubularin has been reported to act on the phosphatidylinositol 3-phosphate/phosphatidylinositol 3-kinase pathway (56), which leads to stimulation of Rac1 (57) and is required for cell transformation induced by Tax (58). Finally, spot 29 contains three Armadillo/β-catenin-like repeats ($E = 0.019$ in BLAST), which are involved in mediating interaction of β-catenin with its ligands. Collectively, these data suggest that LIM, SH3, PDZ, coiled-coil, and myotubularin-related structures may be partly sufficient for Tax binding and possibly induce transformation by Tax.

In summary, our data has identified a number of Tax-interacting proteins from a large cellular fraction through the use of a proteomic approach. Although much of the results presented here await further functional analysis, they may help to explain the many reported functional and physical interactions of Tax with signal transduction proteins and transcription factors, which in turn may deregulate normal cellular functions in favor of T-cell transformation and leukemia.

Acknowledgments—We thank Dr. Richard A. Cerione (Dept. of Molecular Medicine, Cornell University, Ithaca, NY) and Dr. Alan Hall (Medical Research Council laboratory for Molecular Cell Biology, University College London, United Kingdom) for the GST-Cdc42hs, RhoA, Rac1, and Tax plasmids, and Dr. Weidong Wang (Laboratory of Genetics, NIA, National Institutes of Health, Baltimore, MD) for antibodies against SWI/SNF components. We also thank Dr. John N. Brady (NCI, National Institutes of Health) for the anti-Tax polyclonal antibody.

REFERENCES

1. Jeang, K. T. (2001) *Cytokine Growth Factor Rev.* **12,** 207–217
2. Burton, M., Upadhyaya, C. D., Maier, B., Hope, T. J., and Semmes, O. J. (2000) *J. Virol.* **74,** 2351–2364
3. Nicot, C., Tie, F., and Giam, C. Z. (1998) *J. Virol.* **72,** 6777–6784
4. Lenzmeier, B. A., Giebler, H. A., and Nyborg, J. K. (1998) *Mol. Cell. Biol.* **18,** 721–731
5. Riou, P., Bex, F., and Gazzolo, L. (2000) *J. Biol. Chem.* **275,** 10551–10560
6. Kwok, R. P., Laurance, M. E., Lundblad, J. R., Goldman, P. S., Shih, H., Connor, L. M., Marriott, S. J., and Goodman, R. H. (1996) *Nature* **380,** 642–646
7. Yan, J. P., Garrus, J. E., Giebler, H. A., Stargell, L. A., and Nyborg, J. K. (1998) *J. Mol. Biol.* **281,** 395–400
8. Hiscott, J., Kwon, H., and Genin, P. (2001) *J. Clin. Invest.* **107,** 143–151
9. Yamaoka, S., Courtois, G., Bessia, C., Whiteside, S. T., Weil, R., Agou, F., Kirk, H. E., Kay, R. J., and Israel, A. (1998) *Cell* **93,** 1231–1240
10. Jin, D. Y., Giordano, V., Kibler, K. V., Nakano, H., and Jeang, K. T. (1999) *J. Biol. Chem.* **274,** 17402–17405
11. Caliendo, A. M., Savara, A., An, D., DeVore, K., Kaplan, J. C., and D'Aquila, R. T. (1996) *J. Virol.* **70,** 2146–2153
12. Chu, Z. L., Shin, Y. A., Yang, J. M., DiDonato, J. A., and Ballard, D. W. (1999) *J. Biol. Chem.* **274,** 15297–15300
13. Harhaj, E. W., and Sun, S. C. (1999) *J. Biol. Chem.* **274,** 22911–22914
14. Xiao, G., Harhaj, E. W., and Sun, S. C. (2000) *J. Biol. Chem.* **275,** 34060–34067
15. Gachon, F., Thebault, S., Peleraux, A., Devaux, C., and Mesnard, J. M. (2000) *Mol. Cell. Biol.* **20,** 3470–3481
16. Yin, M. J., Paulssen, E. J., Seeler, J. S., and Gaynor, R. B. (1995) *J. Virol.* **69,** 3420–3432
17. Harrod, R., Tang, Y., Nicot, C., Lu, H. S., Vassilev, A., Nakatani, Y., and Giam, C. Z. (1998) *Mol. Cell. Biol.* **18,** 5052–5061
18. Jin, D. Y., Teramoto, H., Giam, C. Z., Chun, R. F., Gutkind, J. S., and Jeang, K. T. (1997) *J. Biol. Chem.* **272,** 25816–25823
19. Chun, A. C., Zhou, Y., Wong, C. M., Kung, H. F., Jeang, K. T., and Jin, D. Y. (2000) *AIDS Res. Hum. Retroviruses* **16,** 1689–1694
20. de La Fuente, C., Santiago, F., Chong, S. Y., Deng, L., Mayhood, T., Fu, P., Stein, D., Denny, T., Coffman, F., Azimi, N., Mahieux, R., and Kashanchi, F. (2000) *J. Virol.* **74,** 7270–7283
21. Kashanchi, F., Duvall, J. F., Kwok, R. P., Lundblad, J. R., Goodman, R. H., and Brady, J. N. (1998) *J. Biol. Chem.* **273,** 34646–34652
22. Wang, D., de la Fuente, C., Deng, L., Wang, L., Zilberman, I., Eadie, C., Healey, M., Stein, D., Denny, T., Harrison, L. E., Meijer, L., and Kashanchi, F. (2001) *J. Virol.* **75,** 7266–7279
23. O'Farrell, P. H. (1975) *J. Biol. Chem.* **250,** 4007–4021
24. O'Connell, K. L., and Stults, J. T. (1997) *Electrophoresis* **18,** 349–359
25. Kuo, M. H., and Allis, C. D. (1999) *Methods* **19,** 425–433
26. Vignali, M., Steger, D. J., Neely, K. E., and Workman, J. L. (2000) *EMBO J.* **19,** 2629–2640
27. Kashanchi, F., Duvall, J. F., and Brady, J. N. (1992) *Nucleic Acids Res.* **20,** 4673–4674
28. Li, X. H., Murphy, K. M., Palka, K. T., Surabhi, R. M., and Gaynor, R. B. (1999) *J. Biol. Chem.* **274,** 34417–34424
29. De Valck, D., Jin, D. Y., Heyninck, K., Van de Craen, M., Contreras, R., Fiers, W., Jeang, K. T., and Beyaert, R. (1999) *Oncogene* **18,** 4182–4190
30. Bar-Sagi, D., and Hall, A. (2000) *Cell* **103,** 227–238
31. Carlier, M. F., Ducruix, A., and Pantaloni, D. (1999) *Chem Biol* **6,** R235–240
32. Hassan, A. H., Neely, K. E., and Workman, J. L. (2001) *Cell* **104,** 817–827
33. Workman, J. L., and Kingston, R. E. (1998) *Annu. Rev. Biochem.* **67,** 545–579
34. Xu, X., Heidenreich, O., Kitajima, I., McGuire, K., Li, Q., Su, B., and Nerenberg, M. (1996) *Oncogene* **13,** 135–142
35. Yin, M. J., Christerson, L. B., Yamamoto, Y., Kwak, Y. T., Xu, S., Mercurio, F., Barbosa, M., Cobb, M. H., and Gaynor, R. B. (1998) *Cell* **93,** 875–884
36. Montaner, S., Perona, R., Saniger, L., and Lacal, J. C. (1998) *J. Biol. Chem.*

273, 12779–12785
37. Reddy, T. R., Li, X., Jones, Y., Ellisman, M. H., Ching, G. Y., Liem, R. K., and Wong-Staal, F. (1998) *Proc. Natl. Acad. Sci. U. S. A.* **95,** 702–707
38. Trihn, D., Jeang, K. T., and Semmes, O. J. (1997) *J. Biomed. Sci.* **4,** 47–53
39. Yoshida, M. (1994) *AIDS Res. Hum. Retroviruses* **10,** 1193–1197
40. Salvetti, A., Lilienbaum, A., Portier, M. M., Gounon, P., Paulin, D., and Gazzolo, L. (1993) *Eur. J. Cell Biol.* **61,** 383–391
41. Schmitz, A. A., Govek, E. E., Bottner, B., and Van Aelst, L. (2000) *Exp. Cell Res.* **261,** 1–12
42. Maruta, H., He, H., Tikoo, A., Vuong, T., and Nur, E. K. M. (1999) *Microsc. Res. Tech.* **47,** 61–66
43. Stam, J. C., Michiels, F., van der Kammen, R. A., Moolenaar, W. H., and Collard, J. G. (1998) *EMBO J.* **17,** 4066–4074
44. del Pozo, M. A., Vicente-Manzanares, M., Tejedor, R., Serrador, J. M., and Sanchez-Madrid, F. (1999) *Eur. J. Immunol.* **29,** 3609–3620
45. Fry, C. J., and Peterson, P. K. (2002) *Science* **295,** 1847–1848
46. Jin, D. Y., and Jeang, K. T. (1997) *Nucleic Acids Res.* **25,** 379–387
47. Rousset, R., Fabre, S., Desbois, C., Bantignies, F., and Jalinot, P. (1998) *Oncogene* **16,** 643–654
48. Reynaud, C., Fabre, S., and Jalinot, P. (2000) *J. Biol. Chem.* **275,** 33962–33968
49. Bezprozvanny, I., and Maximov, A. (2001) *Proc. Natl. Acad. Sci. U. S. A.* **98,** 787–789
50. Dawid, I. B., Toyama, R., and Taira, M. (1995) *C. R. Acad. Sci.* (*Paris*) **318,** 295–306
51. Fimia, G. M., De Cesare, D., and Sassone-Corsi, P. (1999) *Nature* **398,** 165–169
52. Fimia, G. M., De Cesare, D., and Sassone-Corsi, P. (2000) *Mol. Cell. Biol.* **20,** 8613–8622
53. Szabo, A., Korszun, R., Hartl, F. U., and Flanagan, J. (1996) *EMBO J.* **15,** 408–417
54. Azuma, T., Witke, W., Stossel, T. P., Hartwig, J. H., and Kwiatkowski, D. J. (1998) *EMBO J.* **17,** 1362–1370
55. Ling, L., and Goeddel, D. V. (2000) *Proc. Natl. Acad. Sci. U. S. A.* **97,** 9567–9572
56. Blondeau, F., Laporte, J., Bodin, S., Superti-Furga, G., Payrastre, B., and Mandel, J. L. (2000) *Hum. Mol. Genet.* **9,** 2223–2229
57. Genot, E. M., Arrieumerlou, C., Ku, G., Burgering, B. M., Weiss, A., and Kramer, I. M. (2000) *Mol. Cell. Biol.* **20,** 5469–5478
58. Liu, Y., Wang, Y., Yamakuchi, M., Masuda, S., Tokioka, T., Yamaoka, S., Maruyama, I., and Kitajima, I. (2001) *Oncogene* **20,** 2514–2526
59. ASP, P., Nihlborg, M., Kalen, M., and Farrants, A. K. (2002) *J. Cell Sci.* **115,** 2735–2746